DYNAMIC MODELING AND CONTROL OF A BALL-JOINT-LIKE VARIABLE-RELUCTANCE SPHERICAL MOTOR

Kok-Meng Lee, Associate Professor and Xiao-an Wang, Graduate Research Assistant

The George W. Woodruff School of Mechanical Engineering
Georgia Institute of Technology
Atlanta, GA 30332-0405

ABSTRACT

This paper presents the dynamic modeling and the control strategy of an interesting three degrees-of-freedom (DOF) variable-reluctance (VR) spherical motor which offers some attractive features by combining pitch, roll, and yaw motion in a single joint. Both the forward dynamics which determine the motion as a result of activating the electromagnetic coils and the inverse model which determines the coil excitations required to generate the desired torque are derived. The model represents the first detailed study on the inverse dynamics, and yet, permits a spectrum of design configurations to be analyzed. The solution to the forward dynamics of the spherical motor is unique but the inverse model may have multiple solutions and therefore an optimal choice is required. The control strategy of a VR spherical motor consists of two parts; namely, the control of the rotor dynamic in terms of the actuating torque, and the determination of the optimal inputs for the required torque. An optimal choice is determined from an unconstrained optimization problem. The implementation issues in determining the optimal control input vector in real-time are also addressed.

1. INTRODUCTION

An increasing need for high performance in robotic applications has motivated several researchers to direct their investigation efforts to new actuator concepts to improve the dexterity of robotic wrists. Examination of the existing mechanical joints reveals that the ball-joint-like spherical actuator is an attractive alternative to the three consecutive-rotational joint configuration. The interest in spherical motor as a robot wrist is triggered because of its ability in providing the roll, yaw, and pitch motion in a single joint, isotropic property in kinematics and kinetics, and its relatively simple structure. Also, it has no singularity in the middle of workspace except at the boundary. The elimination of gears and linkages enables both high positioning precision and fast dynamic response to be achieved. These attractive features have potential applications such as high-speed plasma and laser cutting where the orientation must be achieved rapidly and continuously with isotropic resolution in all directions.

Recently, several design concepts of spherical motor were proposed. A spherical induction motor was conceptualized in [1] for robotic applications and the detailed analysis was given in [2]. However, it is difficult to realize a prototype of its kind because of its complexity in mechanical and winding design and manufacturing, which requires inlaying all three transversing windings on the inner spherical surface of the stator. Laminations are required to prevent movement of unwanted eddy currents. Complicated three phase windings must be mounted in recessed grooves in addition to the rolling supports for the rotor in a static configuration. These and other considerations have led Lee *et al.* [3] to investigate an alternative spherical actuator based on the concept of variable-reluctance (VR) stepper motor which is easier to manufacture. Hollis *et al.* [4] have developed a six DOF direct-current (DC) "magic wrist" as part of a coarse-fine robotic manipulator. An alternative DC spherical motor design with three DOF in rotation was demonstrated by Kanedo *et al.* [5], which can spin continuously and has a maximum inclination of 15°. Although the control of a DC spherical motor is relatively simple, the range of inclination and the torque constant are rather limited. Foggia *et al.* [6] demonstrated an induction type spherical motor of different structure, which has a range of motion characterized by a cone of 60°. Since the control strategy of the induction motor [6] has not been reported, no results were given on the ability of the motor to realize any arbitrary

As compared with its DC counterpart, a VR spherical motor has a relatively large range of motion, possesses isotropic property in motion, and is relatively simple and compact in design. The trade-off, however, is that sophisticated control scheme is require d. In this paper we discuss both the dynamic model and the control strategy of a VR spherical motor. The contributions of this paper may be briefly summarized as follows: (1) An analytical dynamic model of an unique, potentially useful design of a three DOF ball-joint-like VR spherical motor has been described. The model represents the first detailed study on both the forward and the inverse dynamics of a VR spherical motor. Yet, the model permits a spectrum of design configurations to be analyzed; (2) The analysis offers some interesting insights to the design and control of VR spherical motors. For motion control of the VR spherical motor, both the forward dynamics which determine the motion as a result of activating the motor coils and the inverse model which determines the coil excitations required to obtain the desired torques are needed. The solution to the inverse model has multiple solutions and allows an optimal control vector to be chosen to minimize a specified cost function. This characteristic significantly differs from that of a popular three-consecutive-rotational-joint wrist based on the traditional single-axis motor or spherical motors of other types which typically have unique solutions to both the forward and inverse dynamics and therefore limited the flexibility of controller designs; (3) The paper also represents the first attempt to address the control strategy of the VR spherical motor. The formulation of an unconstrained optimization problem from a standard problem of constraint extrema is interesting. The implementation issues are discussed.

2. DYNAMIC MODEL

The VR spherical motor referred to in this paper is a ball-joint-like device similar to that conceptualized by Lee and Kwan [7].

2.1 Structure of a VR Spherical Motor

The structure of the VR spherical motor is shown in Fig. 1 and an exploded assembly view is given in Fig. 2. The VR spherical motor consists of basically three mechanical assemblies; namely, a spherical rotor, a hollow spherical stator, and an orientation measuring system. The spherical rotor is constrained but allowed to roll on the bearing gimbals which are mounted on the inner surface of the stator.

The coils with ferromagnetic cores are evenly located on the rotor and the stator, and each coil can be energized individually. In order to maintain geometrical symmetry for simplicity in control, the stator poles and the rotor poles are of circular shape. The rotor poles meet at the center of the rotor, and the stator cores are connected by the magnetic conductor layer in the stator shell to form a magnetic circuit with the airgap. The poles are evenly spaced on the stator and the rotor following the pattern of regular polyhedrons. Each vertex of the polyhedron corresponds to the location of one pole. It can be shown that the maximum number of coils which can be evenly spaced on a sphere is 20, the figure corresponding to the number of complex angles of a dodecahedron.

In the operation of the VR spherical motor, the stator coils are energized individually using the control circuitry. A magnetic field is established which creates magnetic energy in the airgap. The created energy is a function of the relative position of the rotor and the stator. The motion of the spherical VR motor is thus generated as the rotor tends to move to a position such that the energy in the airgap is minimized. The detailed kinematic relationship which describes the orientation of the rotor as a function of the three encoder readings can be found in reference [8].

2.2 Rotor Dynamics

As shown in Fig. 1, a base Cartesian coordinate frame XYZ is fixed at the center of the spherical stator with the X and Y axes pointing towards the x- and y- encoders and the Z axis pointing toward the open-end of the spherical socket. Similarly, a coordinate frame 123 is assigned to the center of the spherical rotor with the 3 axis pointing along the rotor shaft. As it will be discussed later, the structure of the spherical motor has certain symmetric properties with respect to Z-Y-Z Euler angles, which are greatly exploited in solving the optimal control input for a specified torque. Thus, the orientation of the spherical motor is specified using the Z-Y-Z Euler angles. Given an actuating torque $T = [T_1, T_2, T_3]^T$, the rotor dynamic equations described in terms of Z-Y-Z Euler angles, $q=[\phi, \theta, \phi]^T$, is given as follows:

$$M(q)\ddot{q} + h(q, \dot{q}) = T, \tag{1}$$

where

$$M(q) = \begin{bmatrix} I S_\theta^2 & I C_\theta & 0 \\ -I S_\theta C_\theta & I S_\theta & 0 \\ I_z C_\theta & 0 & I_z \end{bmatrix},$$

$I=I_x=I_y$ and I_z are the moments of inertia about the principles axes,

$$h(q, \dot{q}) = \begin{bmatrix} I(-\ddot{\phi}C_{(\theta+\theta)} + \ddot{\theta}\phi C_\theta) - (I-I_z)(\dot{\phi}S_\theta\dot{\theta} + \dot{\theta}C_\theta)(\dot{\phi}C_\theta + \dot{\phi}) \\ I(\ddot{\phi}S_{(\theta+\theta)}) - \ddot{\theta}\phi S_\theta - (I-I_z)(\dot{\phi}S_\theta C_\theta + \dot{\theta}S_\theta)(\dot{\phi}C_\theta + \dot{\phi}) \\ -I_z\ddot{\phi}S_\theta \end{bmatrix},$$

and $S_{(\cdot)}$ and $C_{(\cdot)}$ denote the trigonometric sine and cosine functions of the angle $(\cdot)$, respectively.

2.3 Torque Generation

The actuating torque of the spherical motor is derived by using a lumped-parameter approach. The linearized model allows the flux flowing through the reluctance of airgaps to be considered separately, and yet permits a wide variety of design configurations to be analyzed.

Electro-magnetic system: In the derivation of the analytical model, the reluctance of the iron core is assumed to be negligible as compared to that of the airgap and thus the energy storage occurs solely in the air gap. The error introduced by this assumption depends on the geometrical dimensions of the structure and the permeability of the material. This error, in general, can be significantly reduced with magnetic materials of high permeability. The spacing between any adjacent rotor poles and that between any adjacent stator poles is assumed to be much larger compared to the airgap. This assumption implies that no leakage flux occurs between adjacent stator (or rotor) poles.

The electro-magnetic system of the VR spherical motor is modelled as shown in Fig. 3 for the derivation of the torque generation. The VR spherical motor consists of m active stator coils and n active rotor coils. In Fig. 3, M_{si} and M_{rj} denote the magneto-motive-forces (mmf's), which are the electrical inputs to the i^{th} stator coil and the j^{th} rotor coil respectively; R_{ij} denotes the reluctance of the airgap between the i^{th} stator coil and the j^{th} rotor coil; and Φ_{ij} is the corresponding flux flowing through R_{ij}. The magnetic potential at the stator shell with respect to that of the center of the rotor is denoted as V in Fig. 3.

With the aid of Fig. 3, the magnetic flux Φ_{ij} can be determined from Equation (2).

$$\Phi_{ij} = P_{ij}\,[M_{si} + M_{rj} - V], \tag{2}$$

where the permeance P_{ij} is the reciprocal of R_{ij}. Since

$$\sum_{i=1}^{m}\sum_{j=1}^{n} \Phi_{ij} = 0, \tag{3}$$

the magnetic potential V can be derived by substituting Φ_{ij} from Equation (2) into Equation (3), which leads to

$$V = \frac{\sum_{i=1}^{m}\sum_{j=1}^{n} P_{ij}\,(M_{si} + M_{rj})}{\sum_{i=1}^{m}\sum_{j=1}^{n} P_{ij}}. \tag{4}$$

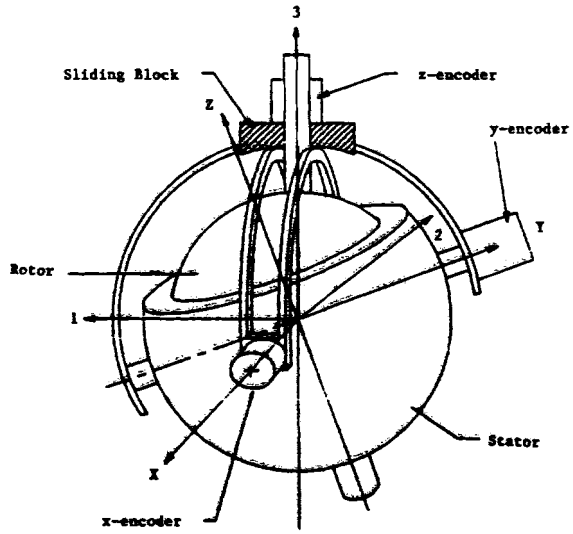

Fig. 1 Structure of a VR Spherical Motor

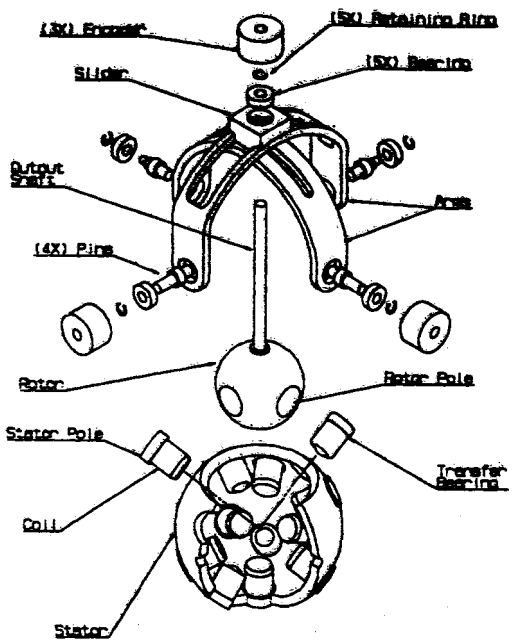

Fig. 2 Assembly View of a VR Spherical Motor

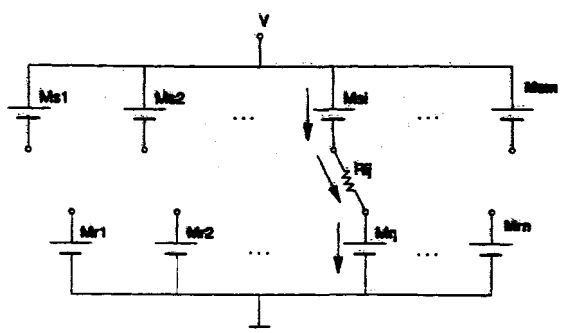

Fig. 3 Magnetic Circuit of the Spherical VR Motor

Governing equations of energy conversion: The torque generated by the electro-magnetic system is derived by using the principle of conservation of energy.

$$\dot{E}_m(t) = \dot{E}_e(t) - T(t) \bullet \omega(t) \tag{5}$$

where

$\dot{E}_m$ = time rate of change of magnetic energy stored,

$\dot{E}_e$ = electrical power input,

T = resultant torque acting on the rotor, and

ω = angular velocity of the rotor.

Since $$T \bullet \omega \, dt = T_x d\phi_x + T_y d\phi_y + T_z d\phi_z \,, \tag{6}$$

where $d\phi_x$, $d\phi_y$ and $d\phi_z$ are the infinitesimal changes of angles with respect to the stator frame. Using the result from Equations (5) and (6) and noting that the differentials of ϕ_x, ϕ_y, and ϕ_z are independent of each other, the torque generated by the magnetic system is given by

$$T = \nabla (E_e - E_m) \,, \tag{7}$$

where

$$\nabla = \left[\frac{\partial}{\partial \phi_x}\right] i + \left[\frac{\partial}{\partial \phi_y}\right] j + \left[\frac{\partial}{\partial \phi_z}\right] k$$

and i, j, k are the unit vectors along the X, Y, Z axes of the stator coordinate, respectively. The electrical power input to the system is given by

$$\dot{E}_e = \sum_{i=1}^{m} \sum_{j=1}^{n} (M_{si} + M_{rj}) \dot{\Phi}_{ij} \tag{8}$$

and the total magnetic energy stored in the system is

$$E_m = \frac{1}{2} \sum_{i=1}^{m} \sum_{j=1}^{n} \Phi_{ij}^2 R_{ij} \,. \tag{9}$$

From Equation (8) and the time-derivative of E_m obtained from Equation (9):

$$\dot{E}_e - \dot{E}_m = \frac{1}{2} \sum_{i=1}^{m} \sum_{j=1}^{n} (M_{si} + M_{rj} - V)^2 \dot{P}_{ij} \,. \tag{10}$$

Combining Equations (1), (6), and (10) and noting that ϕ_x, ϕ_y, and ϕ_z are independent, the torque T can be represented by Equation (11).

$$T = \frac{1}{2} \sum_{i=1}^{m} \sum_{j=1}^{n} (M_{si} + M_{rj} - V)^2 \nabla P_{ij} \,. \tag{11}$$

2.4 Permeance Function

Both numerical computation [10] and experimental results [7] have indicated that a typical permeance model P(x) where x is the relative displacement between two poles has the following properties: 1) P(x) is even, positive, and monotonically decreasing to zero as the displacement increases; 2) The derivative of P(x) has a maximum and minimum at $x = \pm x_m$, where x_m is a constant for a given geometry; 3) The value of P(x) at the origin (i.e. when the poles are fully overlapped) can be reasonably well-determined by

$$P(x) = \frac{\mu_o S(x)}{\ell} \tag{12}$$

where μ_o is the permeanability of air; ℓ is the shortest path length between two parallel pole-faces; and S(x) is the overlapping area between the stator and the rotor poles.

For a given geometry, a typical permeance curve which satisfies the above conditions is given as follows:

$$\frac{P(x)}{P(x=0)} = \frac{1}{1 + \chi^2} \tag{13}$$

where $\chi = x/x_o$ and x_o is a constant to be determined. By noting that the corresponding maximum permeance occurs at $x_m = x_o/\sqrt{3}$, the value of x_o can be determined experimentally or from numerical computation such as finite element method. However, the following additional condition must be satisfied in modeling the permeance function for the spherical motor: P(x) must be periodic with a period 2π. Thus, using Fourier series expansion on $[-\pi, \pi]$ and retain the first N terms, the following periodic permeance function can be obtained.

$$P(x) = a_o + \sum_{k=1}^{N} a_k \cos k \, x \,, \tag{14}$$

where the coefficients $(a_0, a_1, \ldots, a_N)$ can be determined from experimental data or from numerical computation. Note that P(x) is an even function and therefore the sine terms vanished.

2.5 Torque Prediction Model

The torque prediction model determines the torque generated by the spherical motor for a given set of input currents applied to the electromagnetic coils. For a specified geometry, the permeance between any pairs of adjacent stator and rotor poles is a function of the angle between the position vectors characterizing of i^{th} stator and the j^{th} rotor poles, ϕ_{ij}. Hence,

$$P_{ij} = P(\phi_{ij}) \,. \tag{15}$$

Let $C_{si}(x_{si}, y_{si}, z_{si})$ and $C_{rj}(x_{rj}, y_{rj}, z_{rj})$ be the position vectors of the i^{th} stator and the j^{th} rotor poles, respectively. The angle between any pairs of stator and rotor poles can be determined from the dot (inner) product of the position vectors C_{si} and C_{rj}; that is

$$\cos(\phi_{ij}) = \frac{C_{si} \bullet C_{rj}}{R^2} \tag{16}$$

where R is the mean radius of a spherical surface separating the pole faces of the stator and rotor. The position vector of the j^{th} rotor coil with respect to the stator coordinate frame is defined by

$$\begin{bmatrix} C_{rj} \\ 1 \end{bmatrix}_{XYZ} = [T] \begin{bmatrix} c_{rj} \\ 1 \end{bmatrix}_{123} \tag{17}$$

where [T] is a homogeneous transformation describing the rotor frame with respect to stator frame, and c_{rj} describe the position vectors of j^{th} rotor pole with respect to the rotor frame. From Equations (7) and (11), it can be shown by using differential geometry that the torque is given by

$$T = \frac{1}{2} \sum_{i=1}^{m} \sum_{j=1}^{n} \left[(M_{si} + M_{rj} - V)^2 \bullet \frac{dP(\phi)}{d\phi}\Big|_{\phi=\phi_{ij}} e_{ij}\right] \,, \tag{18}$$

where e_{ij} is a unit vector perpendicular to the position vectors C_{si} and C_{rj} and can be written as

$$e_{ij} = \frac{C_{si} \times C_{rj}}{R^2 \sin \phi_{ij}} \tag{19}$$

where $C_{si} \times C_{rj}$ denotes the vector cross-product of C_{si} and C_{rj}. Thus, Equation (18), along with Equations (2) and (19) and a permeance model given by Equation (14), defines the torque generated by the spherical motor for a given set of inputs in terms of the magneto-motive-forces (mmf's) of the coils.

3. MOTION CONTROL STRATEGY

The motion control of the VR spherical motor consists of two parts. The first part is to determine the actuating torques of the VR spherical motor so that the motor follows the desired trajectory. The second part determines the optimal electrical inputs to generate the required actuating torque determined by using the control law for tracking the desired trajectory.

3.1 Control of Rotor Dynamics

The control task is to determine the actuating torque so that q will track the desired trajectory q_d. The spherical motor is controlled using the computed torque method [11]. The feedback law is chosen in the form

$$T = M(q) V + h(q, \dot{q}) \,, \tag{20}$$

where $V = [V_\psi, V_\theta, V_\phi]^T$ is the control vector. Using the feedback law given in Equation (20), the closed-loop dynamic equation becomes

$$M\ddot{q} = MV \,.$$

Since $M(q) > 0$ $V\ \theta \neq 0$ and therefore $M^{-1}(q)$ exists $V\ \theta \neq o$, we have

$$\ddot{q} = V \,. \tag{21}$$

Equation (21) represents a linear system with three decoupled second-order subsystems under the control vector V and hence linear control theory can be applied to each of the coordinates separately. As an example, the control vector V may be chosen as

$$V = \ddot{q}_d - K_1 (\dot{q} - \dot{q}_d) - K_2 (q - q_d) \tag{22}$$

where $K_1 = \text{diag}\,[K_{1\psi}\ K_{1\theta}\ K_{1\phi}]$ and $K_2 = \text{diag}\,[K_{2\psi}\ K_{2\theta}\ K_{2\phi}]$. The tracking error $e = q - q_d$ is guaranteed to approach to zero asymptotically if the elements in K_1 and K_2 are all positive.

The inertia matrix M(q) given in Equation (1) is not invertible at $\theta = 0$, which is, in fact, a singular point for the Z-Y-Z Euler angles. At

this singular point, Equation (21) cannot be obtained from Equations (1) and (20). We shall examine the validity of the control law at the singular point, the Euler Equations are rewritten in state-space representation.

$$\dot{X} = f(X, T), \tag{23}$$

where f is known as the vector field in differential equation theory [12].

As $\theta \neq 0$, we have $X = [\psi, \theta, \phi, \dot{\psi}, \dot{\theta}, \dot{\phi}]$

$$f(X, T) = \begin{bmatrix} \dot{\psi} \\ \dot{\theta} \\ \dot{\phi} \\ [I_t \dot{\theta}\dot{\psi}C_\theta + \dot{\phi}) - 2I\dot{\theta}\dot{\psi}C_\theta - T_1 C_\theta + T_2 S_\theta] \frac{1}{I_t} \\ [(I - I_t)\dot{\psi}\dot{\psi}C_\theta + \dot{\phi}) S_\theta - \dot{\psi}\dot{\theta}I_t + T_1 S_\theta + T_2 C_\theta] \frac{1}{I} \\ [I\dot{\theta}\dot{\psi}^2(1 + C_\theta^2) - I_t\dot{\theta}\dot{\psi}C_\theta + \dot{\psi}\dot{\theta})] \frac{1}{I_t} + (T_1 C_\theta - T_2 S_\theta) C_\theta \frac{1}{I I_t} + \frac{T_3}{I_z} \end{bmatrix} \tag{24}$$

As $\theta = 0$, Equation (1) becomes

$$X = [\theta, \psi + \phi, \dot{\theta}, \dot{\psi} + \dot{\phi}]^T$$

$$f(X, T) = \begin{bmatrix} \dot{\psi} + \dot{\phi} \\ \frac{1}{I}(T_1 S_\theta + T_2 C_\theta) \\ \frac{1}{I_z} T_3 \end{bmatrix} \tag{25}$$

If the control torque T is determined by Equation (20), then the right-hand side of Equation (23) is continuous on $\mathbb{D} \subset \mathbb{R}^6 \times \mathbb{R}$, a closed, connected and bounded region. Furthermore, it also satisfies a local Lipschitz condition on $\mathbb{D}$. Then for any $(x_0, t_0) \in \mathbb{D}$, where $x_0 = x(t_0)$, t_0 is the initial time, there exists a unique solution $x(\cdot, t_0, x_0)$ defined over some interval $a < t_0 < b$ with $(x_0, [a, b]) \subset \mathbb{D}$. Moreover, the solution depends continuously on t_0 and x_0. This argument is based on the Picard's Existence and Uniqueness Theorem [12].

The mapping field f in Equation (23) is not continuous as $\theta = 0$ and hence, local Lipschitz condition is not satisfied. In fact, the rotor motion can essentially be described by the two independent variables θ and $\psi+\phi$ at $\theta = 0$ where the precession and the spin axes are aligned and measured about the same axis. The vector field f degenerates from $\mathbb{R}^6$ in Equation (24) to $\mathbb{R}^4$ in Equation (25). Thus, multiple solutions exist at the singular point of the Z-Y-Z Euler angles as there are two independent equations with three variables.

By the physical nature of ball-joint-like spherical motor, the solution to Equation (1) should be continuous. To ensure a smooth motion at ($\theta = 0$), a generalized vector field must be constructed at ($\theta = 0$) such that the vector field of the closed-loop system is continuous for the rotor dynamics given by Equations (24) and (25). Since the possession and spin angles at ($\theta = 0$) can be arbitrarily chosen provided that their sum is uniquely determined by the location of the body, the control vector V in Equation (21) in state-space representation can be treated as a generalized vector field for the state feedback control law defined by Equation (20). With Equation (25a) replaced by Equation (21) at (θ=0), the vector field is continuous over the whole range of motion and satisfies Lipschitz conditions and hence, the unique solution is ensured. Typical simulation results for a rotor of 76.2 mm diameter with design I= 8.0538E-4 Kg-m^2 and I_z=5.3775E-4 Kg-m^2 are shown in Fig. 4.

3.2 Control Input Optimization

The control input optimization is essentially an inverse problem to torque prediction model. The solution to the inverse problem is to compute a set of coil excitations, which is denoted here as a control input vector U, that is required to generate the desired torque T. Unlike the forward torque prediction model which yields an unique torque vector for a specified set of coil excitations, there are generally infinite solutions to the inverse problem of the torque prediction model of a spherical VR motor for a specified torque. For clarity in illustrating the inverse torque model, the following additional

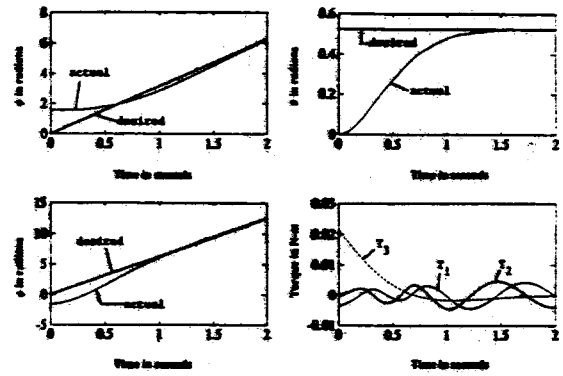

Fig. 4 Simulation Results of Computed Torque Method

assumptions are made: 1) Only current sources are used and the mmf's of the coil are treated as system input variables; 2) In practice, it is desired to have no wiring in the moving parts and thus, only simple iron cores with no excitation coils are assumed as rotor poles (i.e. $M_{ij} = 0, j = 1, \ldots, n$).

Formulation for Inverse Torque Model: In order to choose an optimal solution among many alternatives to the inverse torque model, the torque equation is presented in quadratic form by using the following notations:

$$U = [M_{s1} \ldots M_{sm}]^T \subset \mathbb{R}^m, \tag{26}$$

$$a = [a_1 \ldots a_i \ldots a_n]^T, \tag{27}$$

$$a_i = \frac{\sum_{j=1}^{n} P_{ij}}{\sum_{i=1}^{m}\sum_{j=1}^{n} P_{ij}}, \qquad \sum_{i=1}^{m} a_i = 1 \tag{28}$$

Hence, using the notations defined by Equations (26) to (28), the torque can be written in matrix form as follows:

$$T_I = \frac{1}{2} U^T [A_I] U \qquad I = 1, 2, 3 \tag{29}$$

where

$$[A_I] = \sum_{i=1}^{m} \left| \sum_{j=1}^{n} \frac{dP}{d\phi} \right|_{\phi=\phi_0} (a_0 \cdot u_I) (a - c_i)(a - c_i)^T \tag{30}$$

$$c_i = [0\ 0 \ldots 1\ 0 \ldots 0\ 0] \tag{31}$$

where $(u_I, I=1,2,3)$ is an unit vector along the axes of the rotor body frame. The matrices $[A_I]$, (I=1,2,3) vary with the orientation of the spherical motor.

Given the desired torque, U may be determined from Equation (29) by solving the algebraic equations. However, since $U \in \mathbb{R}^m$ where m is the number of stator coils and is designed larger than three, there are generally infinite numbers of solutions to the inverse problem. It is of interest to determine an optimal solution by some guidelines or a criterion, such as one minimizing of the current amplitude or the consumed power. In other words, the inverse modal is essentially an optimization problem which may be formulated as follows:

$$\text{Minimize } f(U) = \sum_{i=1}^{m} |u_i|^p + M \sum_{I=1}^{3} (\tfrac{1}{2} U^T [A_I] U - T_I)^2 \tag{32}$$

where the weighting factor $M > 0$ is generally a factor very large real number. The generalized reduced gradiate (GRG) method [11], is used to solve for the optimal solution. The minimization of the functional Equation (32) is an unconstrained problem. It has been numerically found that the GRG method works well in minimizing the functional represented by Equation (32).

Illustrative Example: An example is illustrated here by using a design configuration where the stator and the rotor are arranged at the vertices of an icosahedron and a tetrahedron, respectively. However, to allow for the motion of the rotor shaft, only eleven stator poles are used in the design. The characteristic dimensions of the VR spherical motor using in the following example are summarized as follows: The mean radius of the spherical surface separating the stator and the rotor pole faces are 38.1mm. The radius of the stator and the rotor poles is 12.7mm and the airgap separating the stator and the rotor pole faces is 1mm. The permeance model as a function of the relative displacement

between two circular poles was obtained experimentally. The value x_0 in Equation (13) was determined to be 18mm. With the permeance model and the given pole coordinates, the matrices (A_I, I = 1, 2, 3) are formed. To compute for an optimal input mmf's for a specified torque at a given orientation, an initial input mmf's vector is estimated and a local optimal solution is computed by the GRG algorithm. The global optimal solution is then searched by comparing the objective values of local optimal solutions.

As a numerical example, the optimal input mmf's which generate the torque T = 1 u_3 (N-m) at the rotor orientation at (0,0,0) are computed for two cases. In both cases, p is set to be 2 so that the electric power is minimized and by choosing $M = 10^8$ the constraint equations are satisfied with the relative accuracy of 10^{-5}. In case (1), all the eleven input mmf's are independently excited. The values of the optimal input vector is tabulated in TABLE 1. The minimized objective value is 17.8601 and that the absolute value of the maximum input mmf is 3.7816×10^3 Amp-turns.

In case (2), the coil excitations are grouped in pairs so that the number of power amplifiers are reduced. In each grouping, the coils pointing towards each other along a diameter are connected in series, i.e. $u_i = -u_{i+5}$, i = 1, 2,...,5. The optimal solution of case (2) is compared to that of case (1) in TABLE 1. The corresponding objective value is 46.2825 and the absolute value of the maximum mmf is 3.8087×10^3 Amp-turns. Clearly, the additional constraints introduced in case (2) substantially increase the objective value as compared to that in case (1). It is worth noting that the input mmf's can be effectively lowered by reducing the airgap. If the airgap is reduced to 0.01mm, the current amplitudes for the same coils are about 1/10 of the the about results.

Table 1 Simulation Results

pole	case 1 (10^3Amp-turns)	case 2 (10^3Amp-turns)
1	1.5797	0.3167
2	0.2390	-3.5868
3	-1.4074	0.6440
4	-0.4429	-3.8087
5	-3.7816	3.6894
6	1.1861	-0.3167
7	-1.5810	3.6894
8	0.1923	-0.6440
9	-0.2322	3.8087
10	3.4789	-3.6894
11	0.7682	3.0930
Objective Value	17.8601	46.2815

4. CONCLUSIONS

The dynamic model and the control strategy of an innovative three degrees-of-freedom VR spherical motor have been given. The torque prediction model has been derived as a function of the electromagnetic coil excitations and a permeance model as a function of the relative position between the rotor and the stator. The inverse model of a VR spherical motor, which determines the coil excitations for a specified torque, is characterized by its infinite solutions. It has been shown that for a current controlled spherical motor, the relationship between the output torque and the input currents are algebraic and quadratic. The torque prediction model of a current controlled VR spherical motor is decoupled from the dynamic equations of the system, and therefore allows the determination of the optimal electrical inputs to be separated from the motion control of the spherical rotor. Unlike the conventional motor design where the solutions to the forward and inverse models are unique, the multiple-coil excitation allows an optimal control vector to be chosen to minimize a specified cost function in the control of a VR spherical motor.

ACKNOWLEDGEMENTS

This work is supported by the National Science Foundation under grant numbers DMC 8810146 and DDM-8958383. Comments from Professor Y-H Chen of Mechanical Engineering at Georgia Tech are greatly appreciated.

REFERENCES

1. Vachtsevanos, G., and Davey K., and Lee, K.-M. "Development of a Novel Intelligent Robotic Manipulator," IEEE Control Systems Magazine, June 1987.

2. Devay, K. and Vachtsevanos, G. "The Analysis of Fields and Torques in a Spherical Induction Motor," IEEE Trans. on Magnetics, Vol. MAG-23, March 1987.

3. Lee, K.-M., Vachtsevanos, G. and Kwan C-K., " Development of a Spherical Stepper Wrist Motor," Proceedings of 1988 IEEE International Robotics and Automation. Philadelphia, April 25-29, 1988. Also in Journal of Intelligent and Robotic Systems, 225-242 (1988).

4. Hollis, R. L., Allan, A.P. and Salcudan, S., "A Six Degree-of-Freedom Magnetically Levitated Variable Compliance Fine Motion Wrist," Proceedings of the Fourth International Symposium on Robotics Research, Santa Cruz, August 1987.

5. Kaneko, K., Yamada, I., and Itao, K., "A Spherical DC Servo Motor with Three Degrees-of-Freedom," ASME Trans. on Dynamic Systems, Measurement and Control, Vol. III, No. 3, pp. 398-402, September 1989.

6. Foggia, A., Oliver, E., Chappnis, F. and Sabonnadiere, J., "A New Three Degree of Freedom Electromagnetic Actuator," Conference Record - IAS Annual Meeting, Vol. 35, No. 6, Published by IEEE, New York, NY, USA; pp. 137-141, 1988.

7. Lee, K.-M. and Kwan C-K., " Design Concept Development of a Spherical Stepper Wrist Motor," IEEE Journal of Robotics and Automation, Vol. 7, No. 1, pp. 175-181, February 1991.

8. Lee, K.-M. and Pei, J., "Kinematic Analysis of a Three Degrees-of-Freedom Spherical Wrist Actuator," Proceedings of the Fifth International Conference on Advanced Robotics, Pisa, Italy, June 20-22, 1991.

9. Spong, M. and Vidysagar, M., Robot Dynamics and Control, John Wiley and Sons, 1989.

10. Hale, J.K., Ordinary Differential Equations, Krieger, 1980.

11. Wolfe, P., "Methods for Linear Constraints," Nonlinear Programming, North Holland, 1967.